AGU ADVANCING EARTH AND SPACE SCIENCES

JGR Planets

RESEARCH ARTICLE
10.1029/2026JE009725

Key Points:

- High-Mg impact glasses were found in Chang'e-6 lunar soil
- Two of the glasses were transferred from the Apollo basin's peak ring
- The composition of the two glasses indicates KREEP components are locally present on the farside

Supporting Information:

Supporting Information may be found in the online version of this article.

Correspondence to:
L. Zhang and Y.-G. Xu,
zhangle@gig.ac.cn;
yigangxu@gig.ac.cn

Citation:
Zhang, L., Chen, J., Cui, Z., Qian, Y., Wang, C., Chen, Z., et al. (2026). KREEP-bearing noritic lower crust under Apollo basin: Constraints from high-Mg impact glasses in Chang'e-6 soil. *Journal of Geophysical Research: Planets*, *131*, e2026JE009725. https://doi.org/10.1029/2026JE009725

Received 12 FEB 2026
Accepted 7 JUN 2026

KREEP-Bearing Noritic Lower Crust Under Apollo Basin: Constraints From High-Mg Impact Glasses in Chang'e-6 Soil

Le Zhang[1], Jingyou Chen[1], Zexian Cui[1], Yuqi Qian[2], Chengyuan Wang[1], Zhiming Chen[1], Pengli He[1], Fangfang Huang[1], Qing Yang[1], Jintuan Wang[1], Linli Chen[1], Yan-Qiang Zhang[1], and Yi-Gang Xu[1]

[1]State Key Laboratory of Deep Earth Processes and Resources, Guangzhou Institute of Geochemistry, Chinese Academy of Sciences, Guangzhou, China, [2]Department of Earth and Planetary Sciences, GIGCAS-HKU Joint Laboratory of Chemical Geodynamics, The University of Hong Kong, Hong Kong, China

Abstract The Moon's crust is proposed to be composed of an anorthositic upper crust and a noritic lower crust. While the upper crust was the result of the floatation of plagioclase crystallized at the late-stage of lunar magma ocean (LMO), the petrogenesis of the lower crust is in debate. In this study, we found three high-MgO impact glasses in the Chang'e-6 lunar soil, one being troctolitic (P032) and other two being noritic (P133 and P138). A combination match suggests P133 and P138 likely originated from the Apollo basin's peak ring, representing lower crust at Apollo basin. The high Mg# and rare earth element signatures of both glasses support a petrogenesis involving the assimilation of KREEP-bearing crust by partial melts derived from early mafic cumulates of the LMO. This study hence indicates that despite the predominant concentration of KREEP material on the lunar nearside, KREEP components are also locally present on the farside.

Plain Language Summary The Moon's crust is thought to have two main layers: an upper crust made of light-colored rock, and a deeper, denser lower crust whose origin is still debated. By studying glass debris formed by meteorite impacts in the soil returned by Chang'e-6 mission from the lunar farside, we have found new clues about this lower crust. The chemical fingerprints of two specific glasses point to the Apollo basin, a giant crater, as their source. There, the impact likely excavated material from the deep crust. The composition of these glasses suggests that the lower crust at Apollo basin formed when magmas from the Moon's interior incorporated a special type of geochemically enriched material known as KREEP. This is surprising because KREEP, which contains heat-producing elements, was previously thought to be concentrated almost exclusively on the lunar nearside. Our discovery shows that KREEP materials, crucial for understanding the Moon's thermal evolution, are also present in localized areas on the farside, changing our global view of the Moon's formation.

1. Introduction

The lunar magma ocean (LMO) model proposes that the Moon had an anorthositic primary crust, which was formed by the floatation of plagioclase crystallized at the late-stage of LMO (Warren, 1985). Such primary lunar crust was subsequently decorated by highland magnesian-suite (Mg-suite, 4.37–4.1 Ga), alkali-suite (4.37–3.8 Ga), and mare basalts (4.0 Ga−1.0 Ga) globally (Elardo et al., 2023). Thus, the investigation of the lunar crust is crucial to understand the evolution of LMO and the post-LMO magmatism. Seismic velocity studies suggested a stratified structure for the lunar crust with a seismic discontinuity at ca. 20-km (Khan et al., 2000; Wieczorek & Phillips, 1997) separating the anorthositic upper crust and a more mafic lower crust (Lognonné et al., 2003; Wieczorek & Zuber, 2001). However, how the stratified crust formed is in debate and might include: cumulate floatation in LMO (Wieczorek & Zuber, 2001) and emplacement of mafic magma beneath anorthositic crust (Shearer et al., 2015; Walker, 1983). Giant impact craters, penetrating through the crust, may excavate deep crustal and even mantle materials to lunar surface (Baker & Head, 2015; Klima et al., 2011), which might be collected by human's lunar exploration missions.

The Chang'e-6 (CE-6) mission landed on the southern mare of the Apollo basin (Figure 1), which is located at the northeast of the South Pole-Aitken (SPA) basin (Li et al., 2024). The Apollo basin is an ancient (4.16–3.9 Ga; Chen, Zhang, Cui, et al., 2025; Orgel et al., 2018; Potter et al., 2018) peak ring basin with diameters of 247 and 492 km for the inner and outer rings. It was suggested that the Apollo basin was produced by a 40 km-diameter meteorite impact into a 20–40 km-thick crust with a speed of 15 km/s (Potter et al., 2018). Such an impact excavated materials down to a depth of ~30 km, and exposed them on the peak ring (Moriarty et al., 2021; Potter

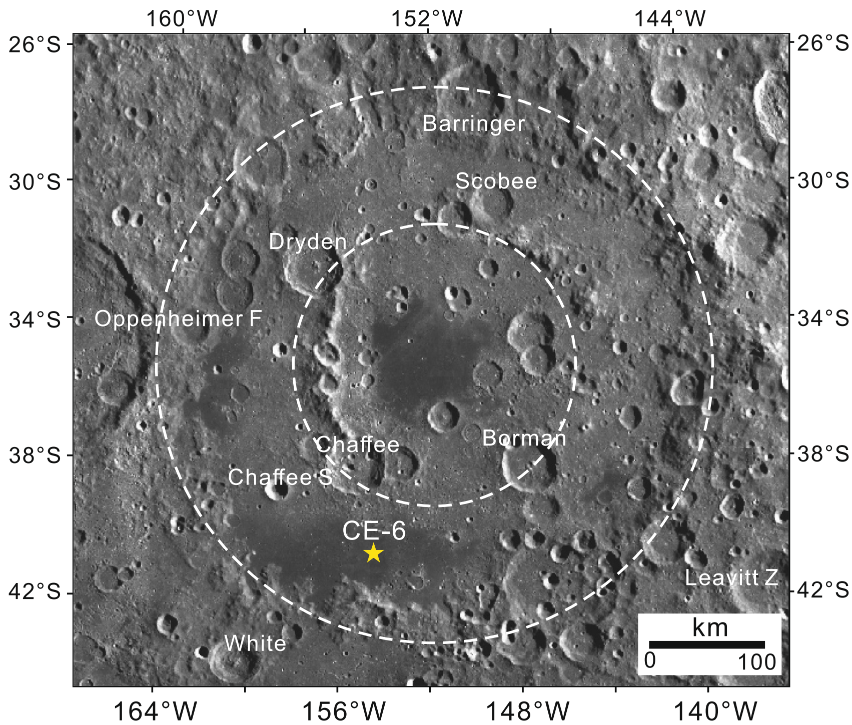

Figure 1. Apollo basin and the Chang'e 6 landing site (yellow star). The white dashed lines mark the Apollo basin rings. The basemap is a LROC WAC image.

et al., 2018). The remote sensing data show that the peak ring of the Apollo basin is characterized with strong absorption features for low-Ca pyroxene, corresponding to a noritic composition (Jia et al., 2024; Qian et al., 2024). It is possible that after the formation of the ca. 2.8 Ga (Cui et al., 2024) mare basalt where the CE-6 mission landed on, subsequent impacts on Apollo peak ring might deliver these noritic materials to the CE-6 landing site. In this study, we found three olivine-bearing glasses selected from the CE-6 lunar soil. The elemental composition indicates an impact origin for these glasses, and two of them have noritic compositions and possibly came from the peak ring of the Apollo basin.

2. Materials and Methods

The olivine-bearing glasses (hereafter, P032, P133, and P138) studied here were selected from CE-6 scooped samples (CE6C0100YJFM003, CE6C0400YJFM00604) allocated by the China National Space Administration (CNSA). The studied glasses are irregular in shape with a size between 200 and 500 μm (Figure 2). All of them have elongate, skeletal olivine phenocrysts (length/width >6) with proportions of 3.2%, 6.6% and 2.7% for P032, P133 and P138, respectively. P032 has two large (∼100 μm) round olivine crystals, which are surrounded by many tiny (<5 μm) olivine crystals. P138 also contains several euhedral-subhedral grain-shaped olivine

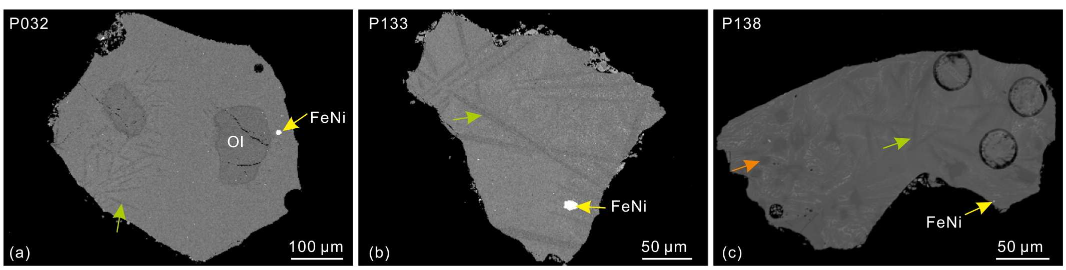

Figure 2. Back-scattered electron images of the three high-MgO glasses from CE-6 lunar soil. All three glasses contain skeletal olivine phenocrysts (green arrows). P032 has two large anhedral olivine and P138 has several euhedral-subhedral grain-shaped olivine (orange arrow). Mineral abbreviation: Ol, olivine; FeNi, FeNi alloy.

(10–20 μm in size). The matrix of P133 and P138 are composed of very fine olivine crystals (1–2 μm) and quenched glass. FeNi alloy occurs in all these glasses.

Back-scattered electron images of the samples were obtained using a Carl Zeiss SUPRA55 SAPPHIRE field emission scanning electron microscope equipped with an Oxford Inca250 X-Max20 energy dispersive spectroscopy system at Guangzhou Institute of Geochemistry, Chinese Academy of Sciences. The accelerating voltage was set to 20 kV.

Elemental compositions of the relatively large grain-shaped olivine in P032 and P138 were measured with a CAMECA SXFive field emission electron probe microanalyzer (EPMA) following the analytical procedural reported in He et al. (2021). The used operation conditions included: 20 kV accelerating voltage, 100 nA beam current, and 2 μm beam size. Under such operation conditions, the detection limits for Al, Ni, and P are ∼30, 80, and 60 ppm, respectively. An olivine reference material MongOl was measured with samples to evaluate the analytical precision. Seven analyses of MongOl during our experiment yielded relative standard deviations (2RSD) of 0.2%–0.5% for SiO_2, MgO, and FeO, ∼5%–8% for MnO, CaO, and Al_2O_3, and ∼10%–15% for NiO and P_2O_5.

As the matrixes of these glasses have crystallized, the major and trace elements of these glasses were measured with a laser ablation system (Resolution M-50, Resonetics) coupled to a sector field inductively coupled plasma mass spectrometer (ELEMENT XR, Thermo Fisher; LA-SF-ICP-MS) following the method outlined by L. Zhang et al. (2019). The laser conditions were as follows: 45 μm beam size, 6 Hz repetition rate and ∼4 J cm^{-2} energy density. Each analysis consisted of 30 s of gas blank data collection with the laser off, and 30 s of sample data acquisition with the laser on. The oxide molecular yield, indicated by $^{232}Th^{16}O/^{232}Th$, was <0.3%. Signals of the following masses were detected: ^{7}Li, ^{23}Na, ^{25}Mg, ^{27}Al, ^{29}Si, ^{31}P, ^{39}K, ^{43}Ca, ^{45}Sc, ^{49}Ti, ^{53}Cr, ^{55}Mn, ^{57}Fe, ^{59}Co, ^{60}Ni, ^{63}Cu, ^{66}Zn, ^{85}Rb, ^{88}Sr, ^{89}Y, ^{90}Zr, ^{93}Nb, ^{95}Mo, ^{133}Cs, ^{137}Ba, ^{139}La, ^{140}Ce, ^{141}Pr, ^{146}Nd, ^{147}Sm, ^{151}Eu, ^{157}Gd, ^{159}Tb, ^{162}Dy, ^{165}Ho, ^{166}Er, ^{169}Tm, ^{174}Yb, ^{175}Lu, ^{178}Hf, ^{181}Ta, ^{208}Pb, ^{232}Th, and ^{238}U. A calibration line for each element was constructed by analyzing two USGS basaltic reference glasses (BHVO-2G, and GSD-1G). The final content of each element was calibrated by normalizing all the measured metal oxides to 100 wt.%. USGS basaltic glass BCR-2G was measured as unknown sample to evaluate the data quality. For most measured elements, the accuracy is better than ±8% with an analytical precision of better than 10%.

3. Results

3.1. Olivine Composition

Nine EPMA analyses on seven euhedral-subhedral olivine phenocrysts in P138 show a relatively homogenous composition with Fo contents (Mg/(Mg + Fe) * 100 in molar) ranging form 90.9 to 93.7, and large variations in CaO (0.17–0.36 wt.%) and Ni (170–528 ppm, Figures 3a and 3b; Table S1 in Supporting Information S1). Two big anhedral olivine crystals in P032 have slightly lower Fo contents (87.9 ± 0.8, 2SD) than olivine in P138. Their CaO (0.048–0.154 wt.%) and Cr_2O_3 (0.012–0.036 wt.%) contents are much lower than in P138 (Figure 3c). On the Mn versus Fe plot, both P032 and P138 are located in the lunar olivine field (Figure 3d).

3.2. Glass Composition

All the three glasses show high MgO (15.4–19.2 wt.%) and Al_2O_3 (17.5–20.8 wt.%), low FeO (6.26–7.37 wt.%) and TiO_2 (0.05–0.22 wt.%), which are significantly different from the mare basalts at the CE-6 landing site (Table S3 in Supporting Information S1; Figure 4). Mare basalts have much higher FeO and, lower Al_2O_3 and Mg# than the studied glasses (Figures 4a–4d). Their compositions are also different from lunar picritic volcanic glasses and dunite, which respectively have much higher FeO and MgO contents. All the three CE-6 high-MgO glasses have high Mg# (Mg/(Mg + Fe) in molar) and moderate FeO, showing affinity with Mg suite (norite and troctolite). While P133 and P138 have nearly the same major elemental composition, P032 has higher Al_2O_3, and lower SiO_2 and TiO_2. Since olivine skeleton crystals in P133 and P138 are quite small compared to a 45 μm laser beam size, the analytical results can represent the bulk compositions of the two clasts. In general, P133 and P138 resemble noritic compositions (e.g., Apollo sample 78237), which are characterized with high Mg#. P032 contains two relative large olivine grains and the bulk composition of P032 was estimated by adding olivine composition into the glass matrix (Table S2 in Supporting Information S1). The proportion of olivine in P032 was estimated by their areas. After this calculation, P032 shows a troctolitic composition (e.g., Apollo sample 76536, Table S3 in

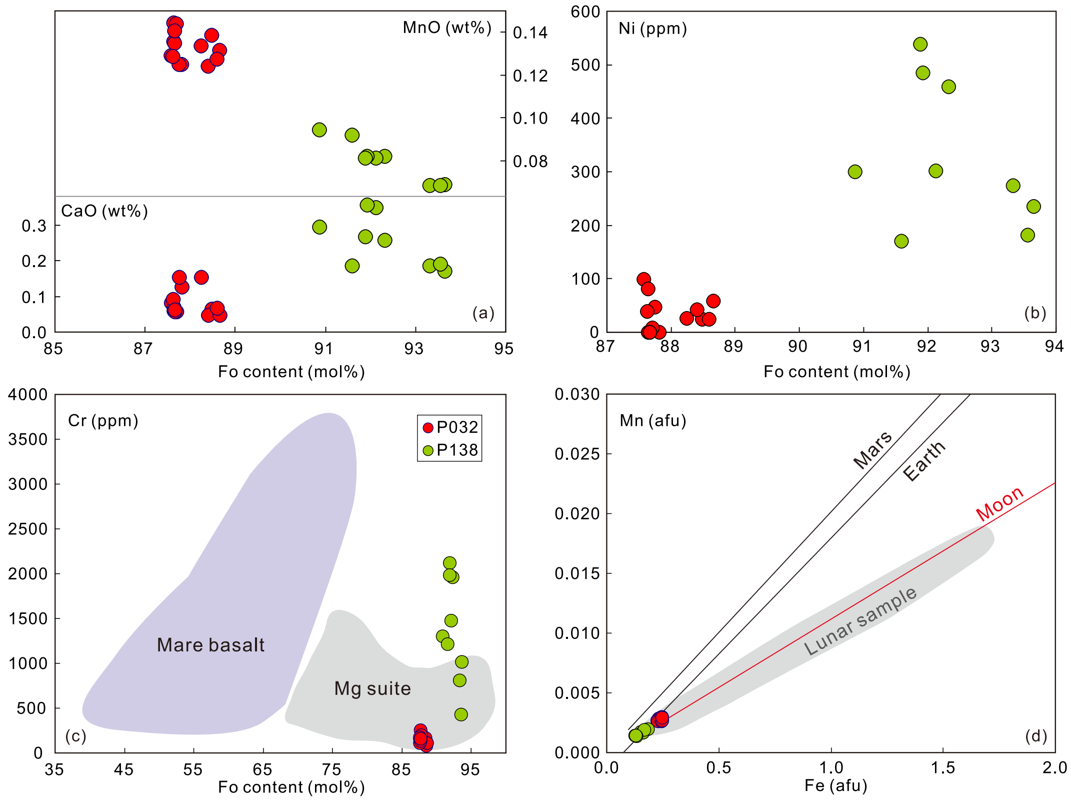

Figure 3. Elemental compositions of olivine from P032 and P138. (a) CaO and MnO versus Fo content plot; (b) Ni versus Fo content plot; (c) Cr versus Fo content plot, the composition fields of mare basalt and Mg suite are from Shearer et al. (2015); (d) Mn versus Fe atoms per formula unit, composition field and trends are from Joy et al. (2014).

Supporting Information S1; Figure 4). In the Mg# versus Ca# (Ca/(Ca + Na + K) in molar) plot (Figure 4c), P133 and P138 are in the range of norites and P032 is in the range of troctolite.

P133 and P138 have similar and relatively high rare earth element (REE) contents ca. 20 times of CI chondrite, in the range of norites (Figure 5). They also show moderate depletion of Eu ($(Eu/(Sm + Gd))_N$ = 0.65–0.76; the subscript N indicates that the ratio is normalized to CI chondrite). In contrast, P032 has much lower REE contents and show a remarkable positive Eu anomaly ($(Eu/(Sm + Gd))_N = 3.5$), similar to that of typical lunar troctolite.

4. Discussions

4.1. An Impact Origin

Glass is one of the major components in all returned lunar samples and it could be produced by volcanic activity or impact events (Delano, 1986; McKay et al., 1991). The following lines of evidence suggest an impact origin of the studied glasses. First, compared to typical volcanic glass returned by Apollo missions, the three studied glasses have much higher Al_2O_3 and lower FeO, showing strong affinity with highland impact glass (Figure 6). Second, these glasses have higher Ni and Ni/Co than pristine highland rocks (Figure 7), indicating the addition of meteoritic materials during impact, as many meteorites have high Fe and Ni contents. Third, an impact origin is further supported by the presence of FeNi alloys in these glasses (Figure 2).

4.2. Precursor Rocks of the Glasses

Although the CE-6 mission landed on a mare region in the southern Apollo basin, besides mare basaltic clasts, the CE-6 lunar soil contains abundant non-mare materials (Chen, Zhang, Chen, et al., 2025; Chen, Zhang, Cui, et al., 2025; Li et al., 2024; Su et al., 2025), which are exotic ejecta transferred by remote meteoritic impact (Guo et al., 2024; Jia et al., 2024; Qian et al., 2024). Because these CE-6 high-MgO glasses are impact-derived and lack the petrological textures of their precursor rocks, their elemental compositions are used to investigate their

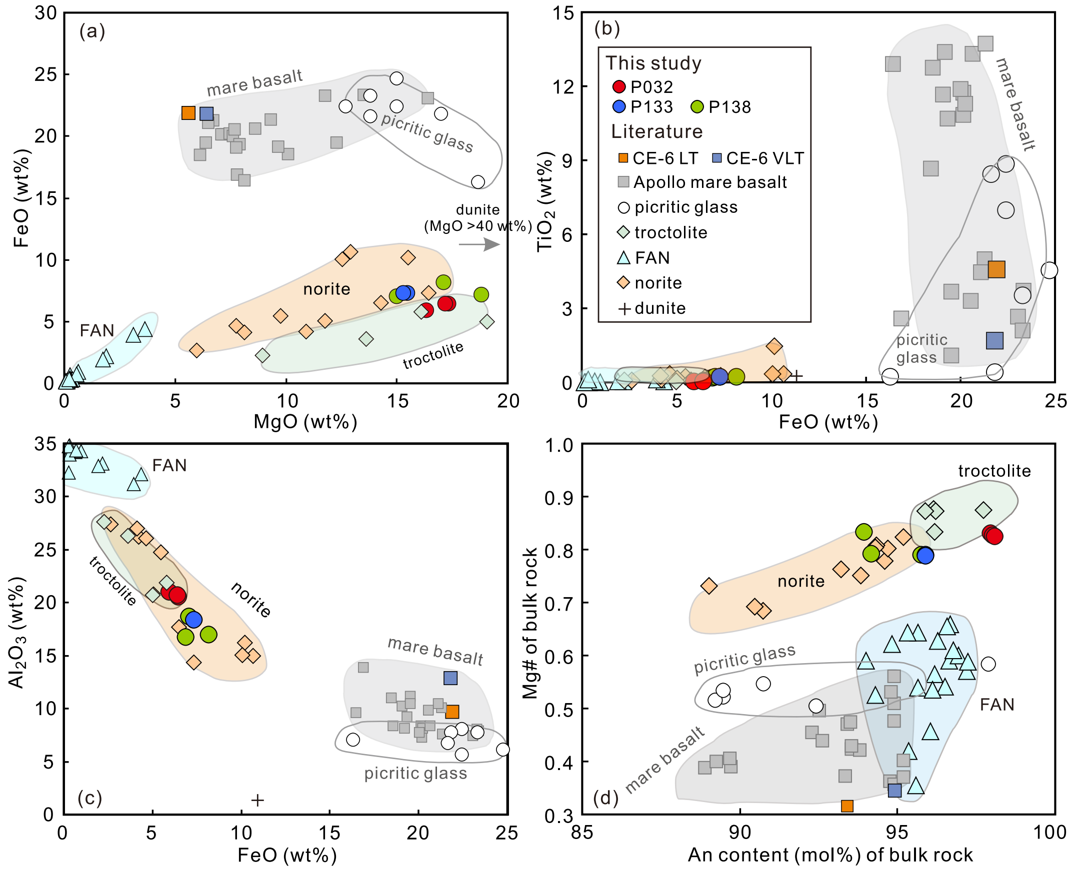

Figure 4. Major element compositions of the CE-6 high-MgO glasses. (a) FeO versus MgO content, (b, c) TiO_2 and Al_2O_3 versus FeO content, (d) Mg# value versus anorthite content. Data of mare basalt, picritic glass, norite, troctolite, and ferroan anorthosite (FAN) are shown for comparison. Data source: FAN, (Dowty et al., 1974; James et al., 1991; Morris et al., 1986; Rose et al., 1973, 1975); Mg suite (norite and troctolite): (Rhodes et al., 1974; Ridley et al., 1973; Warren & Wasson, 1979; Winzer et al., 1974); Apollo mare basalt: compiled by Hallis et al. (2014); Picritic glass: (Delano, 1986; Shearer & Papike, 1993); Dunite: (LSPET, 1973); CE-6 low-Ti (LT) and very-low-Ti (VLT) mare basalt: Wang et al. (2025).

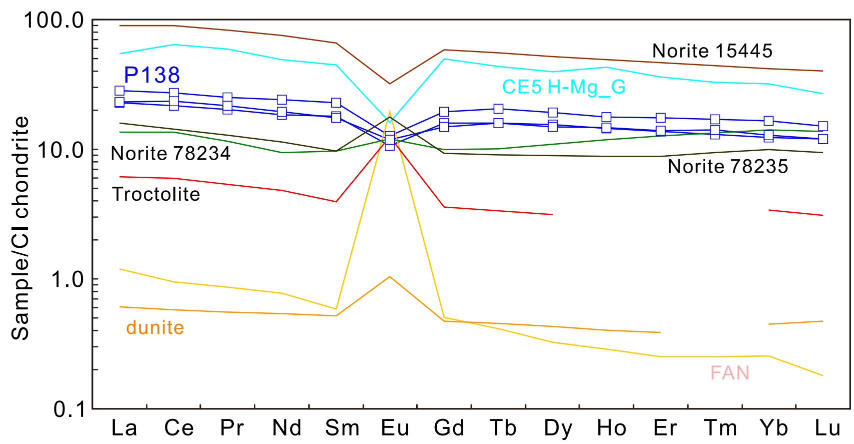

Figure 5. Rare earth element patterns of the CE-6 high-MgO glasses (a) and typical lunar samples (b). Data source: anorthosite, (James et al., 1991); dunite, (Laul & Schmitt, 1973); norite, (Ridley et al., 1973; Winzer et al., 1975); troctolite, (Haskin et al., 1974).

10.1029/2026JE009725

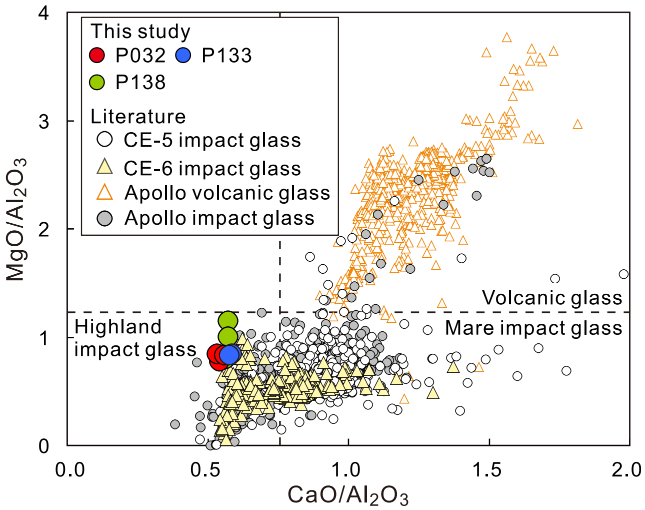

Figure 6. MgO/Al_2O_3 versus CaO/Al_2O_3 plot of lunar glass. The horizontal and vertical dashed lines mark $MgO/Al_2O_3 = 1.25$ and $CaO/Al_2O_3 = 0.75$, respectively (Zeigler et al., 2006). Note that the CE-6 olivine-bearing glasses plot in the highland impact glass range. Reference data of CE-5 and Apollo samples is from the compilation of Wang et al. (2024). CE-6 impact glass is from Chen, Zhang, Chen, et al. (2025).

origins. Olivines in these glasses are extremely fine-grained and exhibit skeletal, needle-like morphologies (Figure 2), indicative of very rapid cooling from a highly superheated melt. Such conditions favor near-complete melting of the precursor. Thus, these impact glasses are compositional representatives of their precursor rocks. As P032, P133, and P138 have quite different chemical compositions from CE-6 mare basalt, all three glasses thus are exotic materials. As mentioned above, the major and trace element compositions indicate P032 has a troctolitic precursor, and P133 and P138 may share a common noritic precursor (Table S3 in Supporting Information S1). The possible origins of these impact glasses were searched by comparing their chemical compositions (FeO, TiO_2 and Th contents) and their precursors' lithologies of potential source craters (Figures S1 and S2 in Supporting Information S1), on the basis of FeO and TiO_2 abundances of Clementine (Lucey et al., 2000) and Th abundance of Lunar Prospector (Prettyman et al., 2006). For P032, the TiO_2, FeO, and Th abundances are set between 0 and 0.5 wt.%, 4.3–8.3 wt.%, and 0–1 ppm, respectively; For P133 and P138, the TiO_2, FeO, and Th abundances are set between 0 and 0.5 wt.%, 5.3–9.3 wt.%, and 0.5–1.5 ppm, respectively, to search for potential source craters for these impact glasses, all based on their measured compositions. In addition, the exposures of olivine (Yamamoto et al., 2012), troctolite (Cahill et al., 2009), and Mg-suite (Prissel et al., 2023) are marked based on previous orbital spectroscopic results to aid the localization of impact source craters.

As the CE-6 mission landed on a mare basalt unit, the impact craters transferred exotic materials to the landing site should have formation ages younger than the southern mare basalt in the Apollo basin. Among possible impact craters, the Chaffee S crater, located on the out edge of the western peak ring of Apollo basin, was suggested to be the most substantial contributor to CE-6 soil with an ejecta thickness of ∼15 cm at the sampling site (Qian et al., 2024). Other impact craters overlaying on the western peak ring of the Apollo basin are either predating CE-6 local mare basalts or too far/small to contribute significant amount of ejecta to the CE-6 sampling site (Figure S3 in Supporting Information S1). The peak ring of Apollo basin is characterized with spectral absorption feature of low-Ca pyroxene and is suggested to have a noritic lithology (Jia et al., 2024; Qian et al., 2024). According to remote sensing studies of Jia et al. (2024) and Guo et al. (2024), the Apollo basin's peak ring has Mg# as high as around 0.8 and FeO ∼8 wt.%, which are quite similar to the compositions of P133 and P138 (Mg# = 0.8, FeO = ∼7.34 wt.%). Therefore, P133 and P138 are most likely ejecta from the Apollo basin's peak ring transferred by the Chaffee S crater-formation impact, to CE-6 soil (Qian et al., 2024).

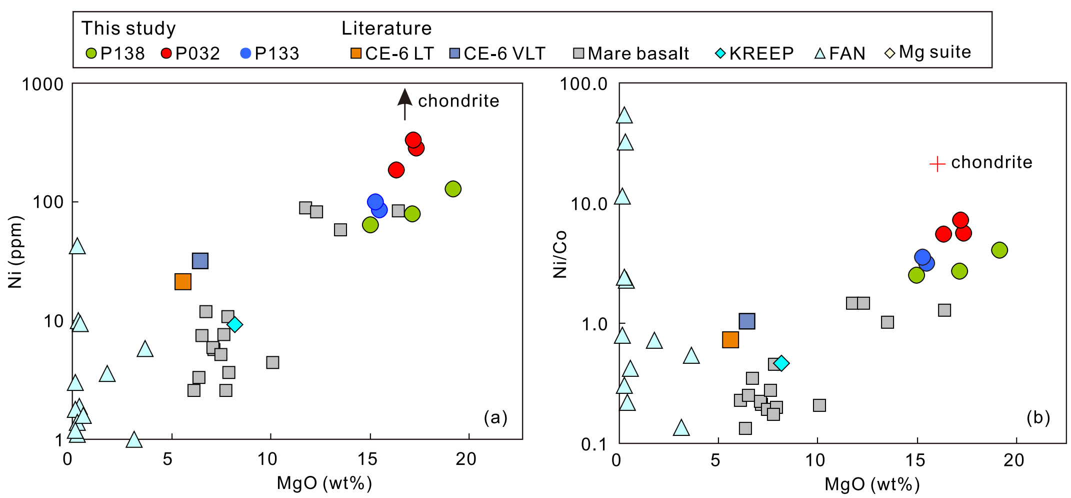

Figure 7. Ni (a) and Ni/Co (b) versus MgO of the CE-6 high-MgO glass. Data source is the same as that in Figure 4. CE-6 LT, CE-6 low-Ti basalt; CE-6 VLT, CE-6 very-low-Ti basalt; FAN, ferroan anorthosite; Mg suite, magnesium suite. The CE-6 olivine-bearing glasses have elevated Ni and Ni/Co compared to ferroan anorthosite and Mg suite.

The chemical composition of P032 and the occurrence of residual olivine indicate a troctolitic precursor. Although the excavation depth of the SPA basin-formation impact was suggested more than 100 km (Potter et al., 2012), possibly excavated upper mantle materials, a very limited olivine signal was detected across the SPA basin (Moriarty et al., 2021; Yamamoto et al., 2012). The remote sensing data also reveal the deficiency of olivine within and around the Apollo basin (Figure S1 in Supporting Information S1; Jia et al., 2024). It was found that some parts of the peak ring of Schrödinger basin and the central peaks of Zeeman crater, which lie about 1,300 and 1,000 km south of the CE-6 landing site respectively, are olivine-rich and have a troctolitic lithology (Figure S2 in Supporting Information S1; Kramer et al., 2013; Yamamoto et al., 2012). However, both the Schrödinger basin and the Zeeman crater have formation ages older than 3.8 Ga in the Nectarian Period (Orgel et al., 2018; Shoemaker et al., 1994), much older than the southern mare of the Apollo basin (Cui et al., 2024). No other large and young crater, which could deliver olivine-rich materials to the CE-6 landing site, was observed in the Schrödinger basin and the Zeeman crater (Poehler et al., 2021). Therefore, although both craters have olivine-bearing lithologies, P032 is unlikely to originate from either of these two craters. Instead, the Lowell crater ($D = 66$ km), which is located in the NW quadrant of Orientale basin, has remote-sensing signal of troctolite with a non-negligible thick ejecta on the CE-6 sampling site (Figure S2 in Supporting Information S1). It was suggested to have a formation age of 374 ± 28 Ma (Srivastava & Varatharajan, 2016), younger than the southern mare of the Apollo basin, and its ejecta thickness is estimated to 1.8 cm at CE-6 landing site based on the ejecta thickness model of (Sharpton, 2014). Thus, P032 was possibly ejected from the Lowell crater.

4.3. Implication for the Composition of the Lower Crust Under Apollo Basin

While the impact glasses P133 and P138 have olivine phenocrysts, remote-sensing data indicate the peak ring of Apollo basin lacks olivine (Figure S3 in Supporting Information S1; Jia et al., 2024; Qian et al., 2024). The glass matrix and the skeleton shape of the olivine phenocrysts (Figure 2) indicate P133 and P138 were quenched soon on lunar surface. It is normally suggested that peak rings represent the deepest materials excavated by an impact basin event that likely reach deep crust (Potter et al., 2018), and high pressure contracts the stability field of olivine while expanding that of pyroxene (Morse, 1980). We thus calculated the phase assemblage of P133 and P138 under different pressure using the petrological modeling program MELTs (Asimow & Ghiorso, 1998) with a fO_2 of IW-1 in a dry system. As P133 and P138 have quite similar chemical composition, we only used the composition of P138 in calculation. Before the calculation, the influence of any meteoritic component on the elemental composition of P138 must be evaluated. P138 has a Ni content of 90.4 ppm, whereas pristine lunar Mg-suite rocks typically contain less than 50 ppm Ni (Edmunson et al., 2009; Rhodes et al., 1974). Assuming Ni contents of 1.0–6.6 wt.% for meteoritic materials (Tagle & Berlin, 2008), the estimated meteoritic contribution to P138 is only about 0.1%–0.9%. Such a low contribution has a negligible effect on the modeling results. Therefore, the composition of P138 was used directly in the modeling. The MELTs phase calculation shows that with increasing pressure from 1 bar to 5 kbar, the proportion of olivine gradually decreases and the proportion of pyroxene (Opx and Cpx) increases (Figure 8). When the pressure is higher than 3.5 Kbar, the proportion of olivine will be less than 10%, which may be difficult for remote sensing detection (Cloutis et al., 1986). Such a pressure roughly corresponds to a 70 km depth, which is consistent with numerical simulation results for a 20 km-thick crust (Potter et al., 2018), indicating a deep-seated origin for the peak ring of the Apollo basin, compositionally recorded in impact glasses P133 and P138.

4.4. Petrogenesis of the Noritic Lower Crust Under the Apollo Basin

Three scenarios are considered for the formation of the noritic lunar crust under the Apollo basin: (a) cumulate floatation during late-stage of LMO; (b) the intrusion and underplating of mafic magma after the consolidation of LMO; (c) cumulates of the SPA impact melt sheet. In the first scenario, during the formation of primary lunar anorthositic crust, floatation of plagioclase crystallized at the late-stage of LMO might bring some co-crystallized mafic minerals (olivine and pyroxene) and incorporate them into the primary lunar crust (Walker, 1983). As floatation of plagioclase started after 70%–80% crystallization of LMO, the co-crystallized mafic minerals should have an evolved composition, (e.g., Mg# < 0.75; Schmidt & Kraettli, 2022), but this is inconsistent with high magnesian olivine composition in P138 (Fo = 90–94). In the third scenario, the SPA basin-formation impact induced melting of the target and formed a 50 km-thick impact melt sheet, like a small magma ocean (Hurwitz & Kring, 2014). The cooling and crystallization of the impact melt sheet produced cumulates with various lithologies, including norite. However, this scenario suffers from the similar problem as in Scenario 1. The SPA impact

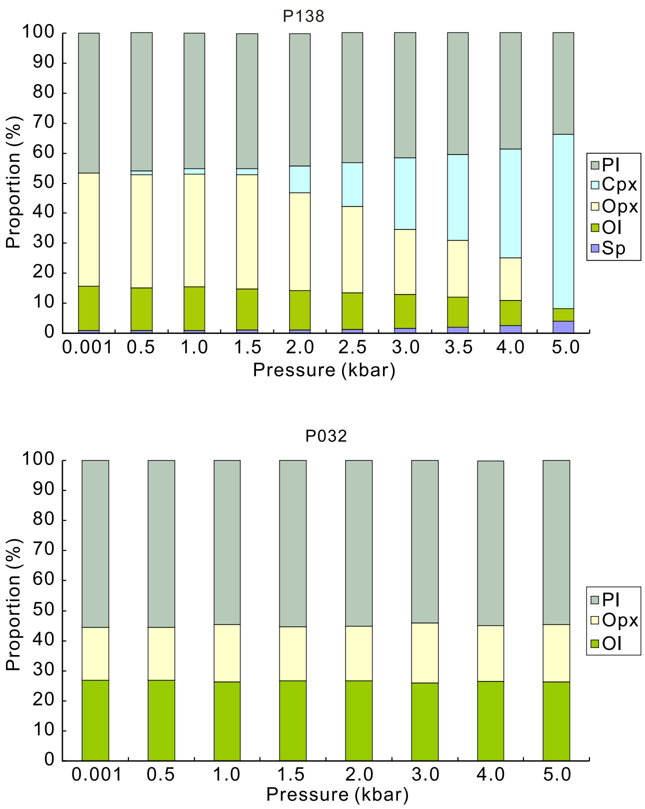

Figure 8. MELTs modeling mineral assemblage of P138 under different pressure. Mineral abbreviation: Pl, plagioclase; Cpx, clinopyroxene; Opx, orthpyroxene; Ol, olivine; Sp, spinel.

excavated material from depths insufficient (80–120 km, Citron et al., 2024) to incorporate primitive high-Mg# mantle cumulates, leading to an impact melt sheet with Mg# possibly as low as 0.5–0.6 (Hurwitz & Kring, 2014), which is too evolved to produce norite with composition like P133 and P138.

In fact, the Mg# of bulk composition of LMO estimated by many studies is about 0.8–0.84 (Elkins-Tanton et al., 2011) and Fo value of the corresponding equilibrated olivine ranges from 92.8 to 94.6 if a *Kd* value $((X_{Fe}/X_{Mg})_{ol}/(X_{Fe}/X_{Mg})_{melt})$ of 0.31 was used (Putirka, 2005). Many models for the generation of Mg-suite involve the interaction between early cumulates of LMO and anorthositic crust with or without urKREEP to account for the high-Mg#, high-Al_2O_3 and elevated incompatible trace elements of Mg-suite (Elardo et al., 2011; Prissel & Gross, 2020; Shearer et al., 2015; Spring et al., 2025). Here we considered the second scenario that during the late-stage overturn of LMO cumulates, the early high-MgO cumulate rose and underwent partial melting, producing picritic melt (Elardo et al., 2011; Shearer et al., 2015). The picritic melt reached the base of primary lunar crust and assimilated anorthosite and urKREEP. A simple mass balance calculation was conducted to reproduce the major and REEs of P138. To satisfy the high-Mg# feature of P138, ~2% partial melt (LPUMi, Mg# = 0.84; Prissel & Gross, 2020) of the assumed lunar primitive upper mantle (LPUM, Mg# = 0.8; Elardo et al., 2011) was used to represent picritic magma from deep mantle (Table S4 in Supporting Information S1). Apollo 16 anorthosite 60,215 (Rose et al., 1975), which consists of nearly pure plagioclase with little mafic minerals (~1 vol.%), and high-K KREEP (Warren, 1989), was selected as a crustal contaminator. The REEs of LPUMi was calculated with the LMO model of Snyder et al. (1992), assuming the first 40% cumulates (olivine) of LMO as the mantle source. Since no REE data is available for 60,215, the REE data of 60,025 was instead used. In our modeling, before assimilating lunar crust, LUPMi experienced ~26% fractional crystallization of olivine. However, as shown in Figure 9a, the evolved mantle-derived melt and anorthosite have much lower REEs than P138, which means only assimilation of anorthosite cannot match high REEs in P138. As a consequence, the crustal contaminator is modified to contain 82% anorthosite and 18% high-K KREEP. After ~30% assimilation of such a crustal contaminator, the calculated melt composition largely fits that of P138 in both major elements and REEs (Table S4 in Supporting Information S1; Figure 9b). Such high assimilation proportion was suggested to be hindered by energy budget limitation (Hess, 1994). The problem could be alleviated if KREEP material is more readily assimilated than anorthosite, thereby reducing the necessary assimilation amount. This is a plausible assumption, as the KREEP material is more fertile and more fusible than anorthosite. To further demonstrate the difference of partial melting behaviors between KREEP and ferroan anorthosite (FAN), their partial melting degrees at various temperatures were modeled by MELTs program (Figure S4 in Supporting Information S1). The modeling results indicate compared to FAN, KREEP materials have substantially lower solidus temperatures and at a given partial melting temperature, KREEP materials have at least 10%–20% higher partial melt degree than FAN. For example, at 1,140°C and 1 Kbar, the partial melting degrees of KREEP and FAN are 50% and 7%, respectively (Figure S4b in Supporting Information S1) and the total assimilation amount will be reduced to ~15% (82% * 7% + 18% * 50%), which is more acceptable when considering energy budget limitation. Overall, a high-Mg# mantle-derived magma must assimilate KREEP materials to acquire high REE contents as observed in P138.

4.5. KREEP Material on the Farside

It is well-known that the Moon's nearside and farside are different in many aspects, such as geomorphology, topography, crustal thickness, volcanic activity and chemical composition, which is termed the Moon's global dichotomy (Head & Wilson, 1992; Wasson & Warren, 1980). The nearside has much higher Th content, a proxy for KREEP, than the farside, indicating a global asymmetric distribution of KREEP. Several possible mechanisms were proposed to account for global asymmetric chemical composition, including asymmetrical crystallization of

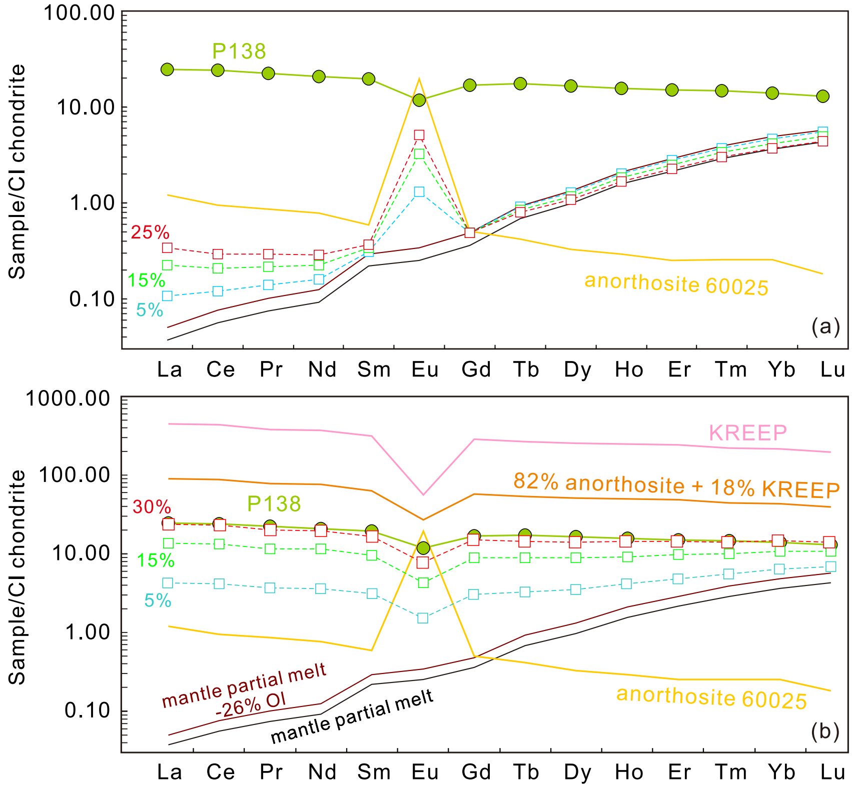

Figure 9. Rare earth element (REE) mass balance modeling of P138. To account for the high REE content in P138, mantle partial melt after 26% crystallization assimilates lunar crust. Dashed lines represent the mixing results. The contaminators compose of 100% anorthosite or 82% anorthosite and 18% KREEP material in (a) and (b), respectively. The numbers besides these dashed lines represent the assimilation degrees of crust. Detailed description of the modeling is described in the main text. Data source is provided in Table S4 in Supporting Information S1.

LMO (Ohtake et al., 2012), an early giant basin-formation impact (Wasson & Warren, 1980; Zhu et al., 2019) and Rayleigh-Taylor instability of lunar mantle after mantle overturn (Zhong et al., 2000). All these mechanisms drove KREEP component to concentrate on lunar nearside. The KREEPy compositional feature of noritic glasses (P133 and P138) found in this study indicates KREEP component still existed below the Apollo basin at ~4.16 Ga (Chen, Zhang, Cui, et al., 2025). Chen, Zhang, Cui, et al. (2025) found three KREEPy impact melt rock clasts in the CE-6 lunar soil, which resulted from the differentiation of SPA basin impact melt pool, and then reworked by the Apollo basin impact. In addition, remote sensing data reveal two thorium "hotspots" (~6 ppm) at craters Birkeland and Oresme V, in northwest of the SPA basin (Moriarty et al., 2021). Interestingly, the recently reported ~2.8 Ga CE-6 low-Ti mare basalt from southern Apollo basin has a KREEP-depleted mantle source (Cui et al., 2024). Since the 4.2 Ga high-Al lavas from the CE-6 landing site has a KREEP signature (Q. W. L. Zhang et al., 2025), it can be inferred that the lunar compositional dichotomy cannot be related to asymmetrical crystallization of LMO. More likely, most KREEP materials have been driven to the nearside by SPA impact, or have been squeezed into SPA impact melt sheets, both leaving behind a very depleted mantle source, from which the 2.8 Ga CE-6 mare basalts were derived (Cui et al., 2024). Nevertheless, this study shows the local presence of KREEP-bearing lower crust beneath the farside.

5. Conclusions

This study identified three high-MgO impact glasses (P032, P133, and P138) in CE-6 lunar soil. Specifically, P032 has a troctolite-like precursor, while P133 and P138 have a norite-like precursor. P032 was possibly transferred from the Lowell crater located to the NW of Orientale basin, whereas P133 and P138 likely originated from the Apollo basin's peak ring and were transferred to the CE-6 landing site by the Chaffee S crater impact. Therefore, P133 and P138 are good representatives of the lower crust below the Apollo basin. The high Mg# of P133 and P138 favors a petrogenetic model of assimilation of anorthositic crust with minor KREEP component by partial melts of deep cumulates of LMO. The presence of the KREEP component in these samples demonstrates that, although most lunar KREEP material is concentrated on the nearside, a small amount of KREEP remains heterogeneously distributed on the farside.

Conflict of Interest

The authors declare no conflicts of interest relevant to this study.

Availability Statement

All the data measured in the study are provided at Mendeley repository (L. Zhang, 2026).

Acknowledgments
This study is financially supported by the Lunar Research Program of the Guangzhou city program (2025A04J7199), GIGCAS (2022SZJJZD-03), the Chinese Academy of Sciences (Grants ZDBS-SSW-JSC007-11, QYJ-2025-0104), Guangdong Basic and Applied Basic Research Foundation (2025A1515010132), and the National Natural Science Foundation of China (42573021, 42241104). Y.Q. is supported by the RGC Co-funding Mechanism on Joint Laboratories with CAS (JLFS/P-702/24) and HK RGC GRF (17307025). The China National Space Administration (CNSA) is appreciated for providing the CE-6 samples. This manuscript benefited much from the constructive comments and suggestions from two anonymous reviewers. This is contribution No. IS-3811 from GIGCAS.

References

Asimow, P. D., & Ghiorso, M. S. (1998). Algorithmic modifications extending MELTS to calculate subsolidus phase relations. *American Mineralogist*, *83*(9–10), 1127–1132. https://doi.org/10.2138/am-1998-9-1022

Baker, D. M. H., & Head, J. W. (2015). Constraints on the depths of origin of peak rings on the Moon from Moon Mineralogy Mapper data. *Icarus*, *258*, 164–180. https://doi.org/10.1016/j.icarus.2015.06.013

Cahill, J. T. S., Lucey, P. G., & Wieczorek, M. A. (2009). Compositional variations of the lunar crust: Results from radiative transfer modeling of central peak spectra. *Journal of Geophysical Research*, *114*(E9). https://doi.org/10.1029/2008JE003282

Chen, J., Zhang, L., Cui, Z., Chen, Z., Xiao, Z., Luo, F., et al. (2025). KREEP-like lithologies in the South Pole–Aitken basin reworked by the Apollo basin impact at 4.16 Ga. *Nature Astronomy*, *9*(11), 1638–1647. https://doi.org/10.1038/s41550-025-02640-5

Chen, Z., Zhang, L., Chen, J., Wang, C., Wang, J., Cui, Z., et al. (2025). Abundant non-mare components in the Chang'e-6 lunar regolith: Constraints from plagioclase fragments and impact glasses. *Journal of Geophysical Research: Planets*, *130*(9), e2025JE008976. https://doi.org/10.1029/2025JE008976

Citron, R. I., Smith, D. E., Stewart, S. T., Hood, L. L., & Zuber, M. T. (2024). The south pole-aitken Basin: Constraints on impact excavation, melt, and ejecta. *Geophysical Research Letters*, *51*(14), e2024GL110034. https://doi.org/10.1029/2024gl110034

Cloutis, E. A., Gaffey, M. J., Jackowski, T. L., & Reed, K. L. (1986). Calibrations of phase abundance, composition, and particle size distribution for olivine-orthopyroxene mixtures from reflectance spectra. *Journal of Geophysical Research*, *91*(B11), 11641–11653. https://doi.org/10.1029/JB091iB11p11641

Cui, Z., Yang, Q., Zhang, Y. Q., Wang, C., Xian, H., Chen, Z., et al. (2024). A sample of the Moon's far side retrieved by Chang'e-6 contains 2.83-billion-year-old basalt. *Science*, *386*(6728), 1395–1399. https://doi.org/10.1126/science.adt1093

Delano, J. W. (1986). Pristine lunar glasses: Criteria, data, and implications. *Journal of Geophysical Research*, *91*(B4), 201–213. https://doi.org/10.1029/JB091iB04p0D201

Dowty, E., Prinz, M., & Keil, K. (1974). Ferroan anorthosite: A widespread and distinctive lunar rock type. *Earth and Planetary Science Letters*, *24*(1), 15–25. https://doi.org/10.1016/0012-821X(74)90003-X

Edmunson, J., Borg, L. E., Nyquist, L. E., & Asmerom, Y. (2009). A combined Sm–Nd, Rb–Sr, and U–Pb isotopic study of Mg-suite norite 78238: Further evidence for early differentiation of the Moon. *Geochimica et Cosmochimica Acta*, *73*(2), 514–527. https://doi.org/10.1016/j.gca.2008.10.021

Elardo, S. M., Draper, D. S., & Shearer, C. K. (2011). Lunar Magma Ocean crystallization revisited: Bulk composition, early cumulate mineralogy, and the source regions of the highlands Mg-suite. *Geochimica et Cosmochimica Acta*, *75*(11), 3024–3045. https://doi.org/10.1016/j.gca.2011.02.033

Elardo, S. M., Pieters, C. M., Dhingra, D., Hanna, K. L. D., Glotch, T. D., Greenhagen, B. T., et al. (2023). The evolution of the lunar crust. *Reviews in Mineralogy and Geochemistry*, *89*(1), 293–338. https://doi.org/10.2138/rmg.2023.89.07

Elkins-Tanton, L. T., Burgess, S., & Yin, Q.-Z. (2011). The lunar magma ocean: Reconciling the solidification process with lunar petrology and geochronology. *Earth and Planetary Science Letters*, *304*(3), 326–336. https://doi.org/10.1016/j.epsl.2011.02.004

Guo, D., Bao, Y., Liu, Y., Wu, X., Xu, Y., Yang, Y., et al. (2024). Geological investigation of the lunar Apollo basin: From surface composition to interior structure. *Earth and Planetary Science Letters*, *646*, 118986. https://doi.org/10.1016/j.epsl.2024.118986

Hallis, L. J., Anand, M., & Strekopytov, S. (2014). Trace-element modelling of mare basalt parental melts: Implications for a heterogeneous lunar mantle. *Geochimica et Cosmochimica Acta*, *134*, 289–316. https://doi.org/10.1016/j.gca.2014.01.012

Haskin, L., Shih, C.-Y., Bansal, B., Rhodes, J., Wiesmann, H., & Nyquist, L. (1974). Chemical evidence for the origin of 76535 as a cumulate. In *Paper presented at lunar science conference, 5th, proceedings*. Pergamon Press.

He, P.-L., Huang, X.-L., Yang, F., & Wang, X. (2021). Mineralogy constraints on magmatic processes controlling adakitic features of early Permian high-magnesium diorites in the Western Tianshan orogenic belt. *Journal of Petrology*, *61*(11–12), egaa114. https://doi.org/10.1093/petrology/egaa114

Head, J. W., & Wilson, L. (1992). Lunar mare volcanism: Stratigraphy, eruption conditions, and the evolution of secondary crusts. *Geochimica et Cosmochimica Acta*, *56*(6), 2155–2175. https://doi.org/10.1016/0016-7037(92)90183-J

Hess, P. C. (1994). Petrogenesis of lunar troctolites. *Journal of Geophysical Research*, *99*(E9), 19083–19093. https://doi.org/10.1029/94JE01868

Hurwitz, D. M., & Kring, D. A. (2014). Differentiation of the South Pole–Aitken basin impact melt sheet: Implications for lunar exploration. *Journal of Geophysical Research: Planets*, *119*(6), 1110–1133. https://doi.org/10.1002/2013JE004530

James, O., Lindstrom, M., & McGee, J. (1991). Lunar ferroan anorthosite 60025-Petrology and chemistry of mafic lithologies. In *Paper presented at lunar and planetary science conference, 21st, proceedings (A91-42332 17-91), Houston, TX*.

Jia, Z., Chen, J., Kong, J., Qiao, L., Fu, X., & Ling, Z. (2024). Geologic context of Chang'e-6 candidate landing regions and potential non-mare materials in the returned samples. *Icarus*, *416*, 116107. https://doi.org/10.1016/j.icarus.2024.116107

Joy, K. H., Crawford, I. A., Huss, G. R., Nagashima, K., & Taylor, G. J. (2014). An unusual clast in lunar meteorite MacAlpine Hills 88105: A unique lunar sample or projectile debris? *Meteoritics & Planetary Science*, *49*(4), 677–695. https://doi.org/10.1111/maps.12270

Khan, A., Mosegaard, K., & Rasmussen, K. L. (2000). A new seismic velocity model for the Moon from a Monte Carlo inversion of the Apollo lunar seismic data. *Geophysical Research Letters*, *27*(11), 1591–1594. https://doi.org/10.1029/1999GL008452

Klima, R. L., Pieters, C. M., Boardman, J. W., Green, R. O., Head, J. W., III, Isaacson, P. J., et al. (2011). New insights into lunar petrology: Distribution and composition of prominent low-Ca pyroxene exposures as observed by the Moon Mineralogy Mapper (M3). *Journal of Geophysical Research*, *116*(E6), E00G06. https://doi.org/10.1029/2010je003719

Kramer, G. Y., Kring, D. A., Nahm, A. L., & Pieters, C. M. (2013). Spectral and photogeologic mapping of Schrödinger Basin and implications for post-south Pole-Aitken impact deep subsurface stratigraphy. *Icarus*, *223*(1), 131–148. https://doi.org/10.1016/j.icarus.2012.11.008

Laul, J., & Schmitt, R. (1973). Chemical composition of Apollo 15, 16, and 17 samples. In *Paper presented at proceedings of the lunar science conference*.

Li, C., Hu, H., Yang, M. F., Liu, J., Zhou, Q., Ren, X., et al. (2024). Nature of the lunar far-side samples returned by the Chang'E-6 mission. *National Science Review*, *11*(11), nwae328. https://doi.org/10.1093/nsr/nwae328

Lognonné, P., Gagnepain-Beyneix, J., & Chenet, H. (2003). A new seismic model of the Moon: Implications for structure, thermal evolution and formation of the Moon. *Earth and Planetary Science Letters*, *211*(1), 27–44. https://doi.org/10.1016/S0012-821X(03)00172-9

LSPET. (1973). Apollo 17 lunar samples: Chemical and petrographic description. *Science*, *182*(4113), 659–672. https://doi.org/10.1126/science.182.4113.659

Lucey, P. G., Blewett, D. T., & Jolliff, B. L. (2000). Lunar iron and titanium abundance algorithms based on final processing of Clementine ultraviolet-visible images. *Journal of Geophysical Research*, *105*(E8), 20297–20305. https://doi.org/10.1029/1999JE001117

McKay, D. S., Heiken, G. H., Basu, A., Blanford, G., Simon, S., Reedy, R., et al. (1991). *The lunar regolith*. Cambridge University Press.

Moriarty, D. P., Dygert, N., Valencia, S. N., Watkins, R. N., & Petro, N. E. (2021). The search for lunar mantle rocks exposed on the surface of the Moon. *Nature Communications*, *12*(1), 4659. https://doi.org/10.1038/s41467-021-24626-3

Morris, R. V., See, T. H., & Hörz, F. (1986). Composition of the Cayley formation at Apollo 16 as inferred from impact melt splashes. *Journal of Geophysical Research*, *91*(B13), E21–E42. https://doi.org/10.1029/JB091iB13p00E21

Morse, S. A. (1980). *Basalts and phase diagrams*. Springer.

Ohtake, M., Takeda, H., Matsunaga, T., Yokota, Y., Haruyama, J., Morota, T., et al. (2012). Asymmetric crustal growth on the Moon indicated by primitive farside highland materials. *Nature Geoscience*, *5*(6), 384–388. https://doi.org/10.1038/ngeo1458

Orgel, C., Michael, G., Fassett, C. I., van der Bogert, C. H., Riedel, C., Kneissl, T., & Hiesinger, H. (2018). Ancient bombardment of the inner solar System: Reinvestigation of the "Fingerprints" of different impactor populations on the lunar surface. *Journal of Geophysical Research: Planets*, *123*(3), 748–762. https://doi.org/10.1002/2017JE005451

Poehler, C., Ivanov, M., van der Bogert, C., Hiesinger, H., Iqbal, W., Pasckert, J., et al. (2021). A new geological map of the lunar south pole-Aitken Basin Region. In *Paper presented at annual meeting of planetary geologic mappers*. Lunar and Planetary Institute.

Potter, R. W. K., Collins, G. S., Kiefer, W. S., McGovern, P. J., & Kring, D. A. (2012). Constraining the size of the South Pole-Aitken basin impact. *Icarus*, *220*(2), 730–743. https://doi.org/10.1016/j.icarus.2012.05.032

Potter, R. W. K., Head, J. W., Guo, D., Liu, J., & Xiao, L. (2018). The Apollo peak-ring impact basin: Insights into the structure and evolution of the South Pole–Aitken basin. *Icarus*, *306*, 139–149. https://doi.org/10.1016/j.icarus.2018.02.007

Prettyman, T. H., Hagerty, J. J., Elphic, R. C., Feldman, W. C., Lawrence, D. J., McKinney, G. W., & Vaniman, D. T. (2006). Elemental composition of the lunar surface: Analysis of gamma ray spectroscopy data from Lunar Prospector. *Journal of Geophysical Research*, *111*(E12). https://doi.org/10.1029/2005JE002656

Prissel, T. C., & Gross, J. (2020). On the petrogenesis of lunar troctolites: New insights into cumulate mantle overturn & mantle exposures in impact basins. *Earth and Planetary Science Letters*, *551*, 116531. https://doi.org/10.1016/j.epsl.2020.116531

Prissel, T. C., Zhang, N., Jackson, C. R. M., & Li, H. (2023). Rapid transition from primary to secondary crust building on the Moon explained by mantle overturn. *Nature Communications*, *14*(1). https://doi.org/10.1038/s41467-023-40751-7

Putirka, K. D. (2005). Mantle potential temperatures at Hawaii, Iceland, and the mid-ocean ridge system, as inferred from olivine phenocrysts: Evidence for thermally driven mantle plumes. *Geochemistry, Geophysics, Geosystems*, *6*(5). https://doi.org/10.1029/2005gc000915

Qian, Y., Head, J., Michalski, J., Gong, S., Yang, W., Xiao, Z. R. L., et al. (2024). Extensive intrusive magmatism in the lunar Farside Apollo and south pole–aitken basins, Chang'e-6 landing site. *The Astrophysical Journal Letters*, *971*(2), L39. https://doi.org/10.3847/2041-8213/ad698f

Rhodes, J. M., Rodgers, K. V., Shih, C. Y., Bansal, B. M., Nyquist, L. E., Wiesmann, H., & Hubbard, N. J. (1974). The relationships between geology and soil chemistry at the Apollo 17 landing site. In *Paper presented at 5th Lunar Science Conference*. Pergamon Press.

Ridley, W., Hubbard, N., Rhodes, J., Weismann, H., & Bansal, B. J. T. J. O. G. (1973). The petrology of lunar breccia 15445 and petrogenetic implications. *The Journal of Geology*, *81*(5), 621–631. https://doi.org/10.1086/627910

Rose, H., Jr., Baedecker, P., Berman, S., Christian, R., Dwornik, E., Finkelman, R., & Schnepfe, M. (1975). Chemical composition of rocks and soils returned by the Apollo 15, 16, and 17 missions. In *Paper presented at 6th Lunar Science Conference*. Pergamon Press.

Rose, H., Jr., Cuttitta, F., Berman, S., Carron, M., Christian, R., Dwornik, E., et al. (1973). Compositional data for twenty-two Apollo 16 samples. In *Paper presented at proceedings of the lunar science conference*.

Schmidt, M. W., & Kraettli, G. (2022). Experimental crystallization of the lunar magma Ocean, initial selenotherm and density stratification, and implications for crust Formation, overturn and the bulk silicate Moon composition. *Journal of Geophysical Research: Planets*, *127*(5), e2022JE007187. https://doi.org/10.1029/2022JE007187

Sharpton, V. L. (2014). Outcrops on lunar crater rims: Implications for rim construction mechanisms, ejecta volumes and excavation depths. *Journal of Geophysical Research: Planets*, *119*(1), 154–168. https://doi.org/10.1002/2013JE004523

Shearer, C. K., Elardo, S. M., Petro, N. E., Borg, L. E., & McCubbin, F. M. (2015). Origin of the lunar highlands Mg-Suite: An integrated petrology, geochemistry, chronology, and remote sensing perspective. *American Mineralogist*, *100*(1), 294–325. https://doi.org/10.2138/am-2015-4817

Shearer, C. K., & Papike, J. J. (1993). Basaltic magmatism on the Moon: A perspective from volcanic picritic glass beads. *Geochimica et Cosmochimica Acta*, *57*(19), 4785–4812. https://doi.org/10.1016/0016-7037(93)90200-G

Shoemaker, E. M., Robinson, M. S., & Eliason, E. M. (1994). The south pole Region of the Moon as seen by clementine. *Science*, *266*(5192), 1851–1854. https://doi.org/10.1126/science.266.5192.1851

Snyder, G. A., Taylor, L. A., & Neal, C. R. (1992). A chemical model for generating the sources of mare basalts: Combined equilibrium and fractional crystallization of the lunar magmasphere. *Geochimica et Cosmochimica Acta*, *56*(10), 3809–3823. https://doi.org/10.1016/0016-7037(92)90172-F

Spring, I., Mallik, A., Kirk, J., Moitra, P., Hervig, R., & Borg, L. (2025). Trace element analyses of plagioclase from troctolite 76535 and implications for the petrogenesis of the lunar highlands Mg-suite. *Meteoritics & Planetary Science*, *60*(10), 2469–2487. https://doi.org/10.1111/maps.70047

Srivastava, N., & Varatharajan, I. (2016). Geomorphology of Lowell crater region on the Moon. *Icarus*, *266*, 44–56. https://doi.org/10.1016/j.icarus.2015.11.013

Su, B., Chen, Y., Wang, Z., Zhang, D., Chen, H., Gou, S., et al. (2025). South Pole–Aitken massive impact 4.25 billion years ago revealed by Chang'e-6 samples. *National Science Review*, *12*(6), nwaf103. https://doi.org/10.1093/nsr/nwaf103

Tagle, R., & Berlin, J. (2008). A database of chondrite analyses including platinum group elements, Ni, Co, Au, and cr: Implications for the identification of chondritic projectiles. *Meteoritics & Planetary Science*, *43*(3), 541–559. https://doi.org/10.1111/j.1945-5100.2008.tb00671.x

Walker, D. (1983). Lunar and terrestrial crust formation. *Journal of Geophysical Research*, *88*(S01), B17–B25. https://doi.org/10.1029/JB088iS01p00B17

Wang, B.-W., Zhang, Q. W. L., Chen, Y., Zhao, W., Liu, Y., Tang, G. Q., et al. (2024). Returned samples indicate volcanism on the Moon 120 million years ago. *Science*, *385*(6713), 1077–1080. https://doi.org/10.1126/science.adk6635

Wang, C., Qian, Y., Wang, J., Liu, L., Zhang, L., Chen, Z., et al. (2025). The source and thermal driver of young (<3.0 Ga) lunar volcanism. *Science Advances*, *11*(34), eadv9085. https://doi.org/10.1126/sciadv.adv9085

Warren, P. H. (1985). The magma ocean concept and lunar evolution. *Annual Review of Earth and Planetary Sciences*, *13*(1), 201–240. https://doi.org/10.1146/annurev.ea.13.050185.001221

Warren, P. H. (1989). KREEP: Major-element diversity, trace-element uniformity. In *Paper presented at Moon in transition: Apollo 14, KREEP, and evolved lunar rocks*.

Warren, P. H., & Wasson, J. T. (1979). The compositional-petrographic search for pristine nonmare rocks-third foray. In *Paper presented at 10th lunar and planetary science conference*. Pergamon Press.

Wasson, J. T., & Warren, P. H. (1980). Contribution of the mantle to the lunar asymmetry. *Icarus*, *44*(3), 752–771. https://doi.org/10.1016/0019-1035(80)90142-6

Wieczorek, M. A., & Phillips, R. J. (1997). The structure and compensation of the lunar highland crust. *Journal of Geophysical Research*, *102*(E5), 10933–10943. https://doi.org/10.1029/97JE00666

Wieczorek, M. A., & Zuber, M. T. (2001). The composition and origin of the lunar crust: Constraints from central peaks and crustal thickness modeling. *Geophysical Research Letters*, *28*(21), 4023–4026. https://doi.org/10.1029/2001GL012918

Winzer, S., Lum, R., Schuhamann, S., & Philpotts, J. (1975). Large ion lithophile trace element abundances in phases from 78235, 34, A lunar norite cumlate. In *Paper presented at abstracts of the lunar and planetary science conference*.

Winzer, S. R., Nava, D. F., Schuhmann, S., Kouns, C. W., Lum, R. K. L., & Philpotts, J. A. (1974). Major, minor and trace element abundances in samples from the Apollo 17 station 7 boulder: Implications for the origin of early lunar crustal rocks. *Earth and Planetary Science Letters*, *23*(3), 439–444. https://doi.org/10.1016/0012-821X(74)90133-2

Yamamoto, S., Nakamura, R., Matsunaga, T., Ogawa, Y., Ishihara, Y., Morota, T., et al. (2012). Olivine-rich exposures in the South Pole-Aitken Basin. *Icarus*, *218*(1), 331–344. https://doi.org/10.1016/j.icarus.2011.12.012

Zeigler, R. A., Korotev, R. L., Jolliff, B. L., Haskin, L. A., & Floss, C. (2006). The geochemistry and provenance of Apollo 16 mafic glasses. *Geochimica et Cosmochimica Acta*, *70*(24), 6050–6067. https://doi.org/10.1016/j.gca.2006.08.040

Zhang, L. (2026). KREEP-bearing noritic lower crust under Apollo Basin: Constraints from High-Mg impact glasses in Chang'e-6 soil [Dataset]. *Mendeley Data, V3*. https://doi.org/10.17632/j4rfwbpc3p.3

Zhang, L., Ren, Z.-Y., Xia, X.-P., Yang, Q., Hong, L.-B., & Wu, D. (2019). In situ determination of trace elements in melt inclusions using laser ablation inductively coupled plasma sector field mass spectrometry. *Rapid Communications in Mass Spectrometry*, *33*(4), 361–370. https://doi.org/10.1002/rcm.8359

Zhang, Q. W. L., Yang, M. H., Li, Q. L., Liu, Y., Yue, Z. Y., Zhou, Q., et al. (2025). Lunar farside volcanism 2.8 billion years ago from Chang'e-6 basalts. *Nature*, *643*(8071), 356–360. https://doi.org/10.1038/s41586-024-08382-0

Zhong, S., Parmentier, E. M., & Zuber, M. T. (2000). A dynamic origin for the global asymmetry of lunar mare basalts. *Earth and Planetary Science Letters*, *177*(3), 131–140. https://doi.org/10.1016/S0012-821X(00)00041-8

Zhu, M.-H., Wünnemann, K., Potter, R. W. K., Kleine, T., & Morbidelli, A. (2019). Are the moon's nearside-farside asymmetries the result of a giant impact? *Journal of Geophysical Research: Planets*, *124*(8), 2117–2140. https://doi.org/10.1029/2018JE005826